Pomegranate MR image analysis using fuzzy clustering algorithms

Ghobad Moradi[1], Mousa Shamsi[2], Mohammad Hossein Sedaaghi[2], Mohammad Reza Alsharif[3]

(1. *Department of Electrical Engineering, Faculty of Engineering, Islamic Azad University, Ravansar Branch, Kermanshah, Iran*;
2. *Faculty of Electrical Engineering, Sahand University of Technology, Tabriz, Iran;*
3. *Department of Information Engineering, Faculty of Engineering, University of the Ryukyus, Japan*)

Abstract: In this paper, the process of the pomegranate magnetic resonance (MR) images was studied. Its internal structure is composed of tissue and seeds, which indicate the dependency between the maturity and internal quality. The latter properties are important in pomegranate's sorting and cannot be measured manually. In this paper, an automatic algorithm was proposed to segment the internal structure of pomegranates. Since the intensities of the calyx and stem of the pomegranate MR image are closely related to that of the soft tissue, their corresponding pixels are therefore labeled in the same class of the internal soft tissues. In order to solve this problem, the exact shape of the pomegranate is first extracted from the background of the image using active contour models (ACMs). Then, the stem and calyx are removed using morphological filters. We have also proposed an improved version of the fuzzy c-means algorithm (FCM), the spatial FCM (SFCM), for segmentation of MR images of pomegranate. SFCM is realized by incorporating the spatial neighborhood information into the standard FCM and modifying the membership weighting of each cluster. SFCM employs spatial information of adjacent pixels leading to an improvement of the results. It thus outperforms other techniques like FCM, even in the presence of Gaussian, salt and pepper, and speckle noises.

Keywords: MRI, pomegranate, image segmentation, spatial fuzzy c-means, morphological filter

Citation: Moradi, G., M. Shamsi, M. H. Sedaaghi, and M. R. Alsharif. 2012. Pomegranate MR image analysis using fuzzy clustering algorithms. Agric Eng Int: CIGR Journal, 14(3): 152−160.

1 Introduction

Pomegranate is one of the tropical fruits growing widely in Iran, Mediterranean countries, India, some parts of America (California), China, Japan and Russia. It is a kind of domestic Iranian fruit which grows in coastal and mountainous areas (Fadavi, Barzegar and Azizi, 2006). It contains some pharmacological properties including antimicrobials, antivirus, anticancer, potent anti-oxidant and anti-mutagenic effects (Negi, Jayaprakash and Jena, 2003). The high-quality of the product is considered an important factor for normal sales in the market. Having an in-time harvest will improve the quality and the nature of storage life of fresh fruits (Prabhu Desai, 1989). Early harvest may impede the development of the characteristic color, taste and aroma of pomegranates, while late-harvested fruits reveal a reduced-shelf life (Kulkarni and Aradhya, 2005). The segmentation of internal components needs to be as exact as possible. Also, for research purposes such as non-destructive investigation, to determine the ripening index and the percentage of seeds in growth period, bruising, the content of water and sugar, extraction of the fruit's internal structure, i.e. the tissue and the seed is necessary.

In order to achieve this goal, the segmentation of the pomegranate MR images can be helpful (Liang and

Received date: 2011-08-19 **Accepted date:** 2012-04-14
*** Corresponding author: Mousa Shamsi,** Faculty of Electrical Engineering, Sahand University of Technology, Tabriz, Iran. Email: shamsi@sut.ac.ir.

Lauterbur, 2000). The high accuracy of image acquisition, the ability to distinguish internal tissues and imaging in non destructive way are amongst the advantages of the MRI techniques. The first application of MRI in horticultural field was reported by Wang, Wang and Faust (1988), who studied water core in apples. Since then, MRI has been applied as one of the qualitative approaches to detect core breakdown in 'Bartlett' pears (Wang and Wang, 1989), to detect void spaces, worm damage and bruises in fruits (Chen, McCarthy and Kauten, 1989; Zion, Chen and McCarthy, 1995; Saito et al., 1996), water core dissipation in apples (Clark, MacFall and Bieleski, 1998; Clark and Burmeister, 1999), woolly breakdown in nectarines and apples (Sonego et al., 1995; Barreiro et al., 1999; Barreiro et al., 2000), internal browning development in 'Fuji' apples (Gonzalez et al., 2001) and to study the effect of postharvest water loss on kiwi's water status (Burdon and Clark, 2001). In our previous works (Moradi et al., 2010a; Moradi et al., 2010b), automatic algorithms were presented for segmentation of the internal structures of pomegranate. Because of the vitality of segmentation of pomegranate images in trade and export, if the segmentation is done manually and by users, it will have significant disadvantages including time consuming, unrepeatability, dependence on user and high cost. In order to remove the aforementioned disadvantages, it is necessary to design and implement automatic algorithms to segment pomegranate MR images without any need of user's interference. Using computers to implement these algorithms helps the cost and repeatability of the work, and if the results are acceptable it will be preferred to the manual methods.

FCM is an unsupervised clustering method which is used successfully in segmentation and clustering of images (Bezdek, 1981; Moradi et al., 2010a; Moradi et al., 2010b). An image can be represented in various feature spaces. FCM algorithm classifies the image by grouping similar pixels in the feature space into clusters. The clustering algorithm is achieved by iteratively minimizing a cost function. It is dependent on the distance of the pixels to the cluster centers in the feature domain. The spatial relationship of adjacent pixels is an important property that can have a significant role in the efficiency of segmentation. General boundary detection techniques have taken the advantage of the spatial information for image segmentation (Chuang et al., 2006; Moradi et al., 2010b). Since FCM does not use the spatial information, it is sensitive to noises. To solve this problem, we suggest SFCM for segmentation. It modifies FCM by considering the spatial information and altering the membership weighting for every cluster. The proposed algorithm greatly reduces the noise effect.

The article is organized as follows: The proposed algorithm is discussed in Section 2. In Section 4, the experimental results and in Section 5 conclusions are proposed.

2 The proposed algorithm

Figure 1 illustrates the flowchart of the proposed method. The image pixels are segmented based on their intensities. Also the intensities of stem and calyx are both close to the tissue's pixels. Therefore, they are often misclassified as the internal tissues by the segmentation algorithm. Distinction between the fruit and the background on image is the first step when extracting the internal structure of pomegranate. However, the difference between their intensities is too small. Therefore, the fruit's shape cannot be easily separated from the background. So, the logarithmic space is considered for intensity. Then, the fruit's shape is extracted using ACM. The next step is to remove stem and calyx using morphological filtering. Finally, the image is segmented using SFCM.

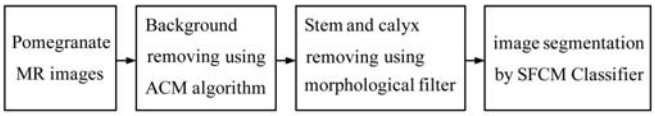

Figure 1 The proposed algorithm

2.1 Image acquisition

Pomegranates from the cultivar 'Malas-e-Torsh' is considered as an important export in Iran. They are almost farmed in Yazd and Saveh. In this research, we have selected two types of pomegranate: semi-ripe and ripe, from orchards of Yazd. Their images were taken in T1, T2 and haste T2 weights. The experiments were

performed on a 1.5T MRI scanner (Siemens, Germany) with two-dimensional spin echo sequence, in the Pejvak Imaging Center, Tabriz, Iran by Dr. Masoud Pour Eisa.

2.2 Pomegranate shape extraction using ACM

Model-based approaches (also called deformable models) are very successful for image interpretation. Among the earliest and most well-known deformable models, the ACM is known as snakes (Kass, Witkin and Terzopoulos, 1988). A snake is an energy minimizing parametric contour that deforms over a series of time steps. Each element along the contour u depends on two parameters where the space parameter $s \in [0, 1]$ is the normalized length around the snake and t is time (iteration):

$$u(s,t) = (x(s,t), y(s,t)) \quad (1)$$

The total energy E_{snake} of the model is computed by the sum of the energy for the individual snake elements:

$$E_{snake} = \int_0^1 E_{element}(u(s,t))ds \quad (2)$$

The energy for each element is decomposed into three basic energy terms:

$$E_{element} = E_{int}(u) + E_{ext}(u) + E_{image}(u) \quad (3)$$

Each point on a contour moves adjacently in order to minimize E_{snake} in each step of the process of repetition. The process stops when a local minimum is met. The internal energy ($E_{internal}$) regulates the constraints arranged on the model tension and stiffness. The external energy ($E_{external}$) is represented by external constraints imposed by high-level sources such as human operators or automatic initialization procedures. The image's energy, E_{image}, drives the model towards the significant features, usually attributed by light and dark lines, edges or terminations. For more details, the reader may refer to Nixon and Aguado (2002).

Figure 2 depicts the result of segmentation using ACM on a pomegranate MR image. To extract the fruit's shape exactly, first, the image intensity is transformed into the logarithmic space as follows:

$$q_{ij} = c.\log(1 + r_{ij}) \quad (4)$$

where, r_{ij} denotes the intensity of the pixel; c is a constant (and is equal to 0.25 in this paper). The original and logarithmic images are illustrated in Figures 2a and 2b, respectively. ACM is applied on Figure 2b. Figures 2c to 2f demonstrate the result for ACM in different iterations, respectively.

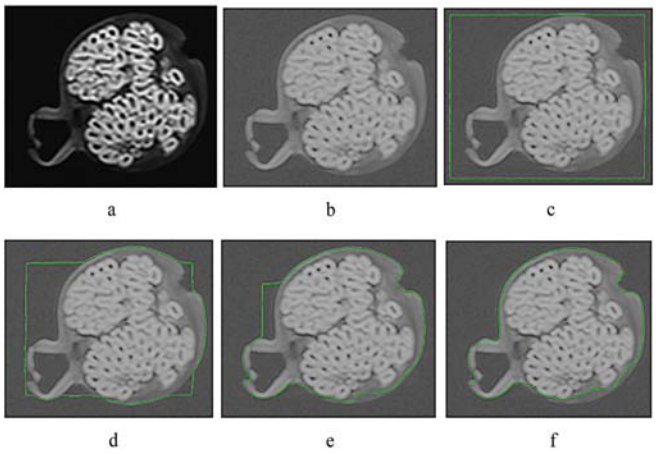

Figure 2 Energy minimization in ACM. a) Original image, b) Logarithmic image, c-f) The result for ACM in different iterations

2.3 Stem and calyx removal using morphological filters

Mathematical morphology represents fundamental theories or the so-called main image operators whose applications can be found by Parvati, Prakasa Rao and Mariya Das (2008). In general, the structural element in a set describes the simple shapes that probe an input image. The basic morphological filters are morphological opening and closing with structuring elements.

In this paper, stem and calyx are removed using opening and closing, which will lead to an exact segmentation of the internal tissue of pomegranate. The opening and closing are applied after the background is removed using ACM and the exact shape of pomegranate is extracted from MR image.

2.4 Image segmentation using fuzzy clustering algorithms

In this section, FCM and SFCM are selected from a set of numerous fuzzy clustering methods to be studied.

2.4.1 FCM clustering algorithm

The FCM, which is an improved version of k-means algorithm, was proposed by Bezdek (1981). It assigns the input feature vectors to each category by using fuzzy memberships. The algorithm is an iterative optimization task which minimizes the cost function defined as follows.

$$J(u,v)=\sum_{i=1}^{c}\sum_{j=1}^{n}\mu_{ij}{}^{m}d^{2}(x_j,v_i) \tag{5}$$

with the following constraints:

$$\sum_{i=1}^{c}\mu_{ij}=1,\quad \mu_{ij}\in[0,1],\quad 1\le j\le n,\quad 1\le i\le c$$

where, $X=(x_1, x_2, \ldots, x_j, \ldots, x_n)$ denotes the input data with a size of $p\times n$, where p represents the dimension of each x_j (feature vector) and n indicates the number of feature vectors, to be partitioned into c cluster. μ_{ij} represents the membership of x_j in the i^{th} cluster, v_i is the i^{th} cluster center, m is a constant. The parameter m controls the fuzziness of the resulting partition (m = 2 is used in this study). d represents the distance between x_j and the cluster center, v_i, i.e.:

$$d^{2}(x_j-v_i)=\|x_j-v_i\|^{2} \tag{6}$$

The objective function is minimized when data points, close to the center of their clusters, are assigned high membership values. Low membership values are assigned to data points far from the centers. The membership functions and the center of the clusters are updated by the following expressions:

$$\mu_{ij}=\left[\sum_{k=1}^{c}\left(\frac{d(x_j,v_i)}{d(x_j,v_k)}\right)^{\frac{2}{m-1}}\right]^{-1} \tag{7}$$

$$v_i=\frac{\sum_{j=1}^{n}\mu_{ij}{}^{m}x_j}{\sum_{j=1}^{n}\mu_{ij}{}^{m}} \tag{8}$$

Starting with an initial guess for the center of each cluster, FCM converges to a solution for v_i representing the local minimum or a saddle point of the cost function. Convergence can be detected by comparing the changes in the membership function or the clusters' center at two successive iterations. Each feature will be associated with a membership value for every class after FCM clustering. The segmentation will be performed by getting the highest membership.

2.4.2 Spatial FCM clustering algorithm

One of the important characteristics of an image is that the neighboring pixels are highly correlated. In other words, they possess similar feature values and the probability of belonging to the same cluster is high. The spatial relationship is important in clustering but it is not taken into account for FCM. To exploit the spatial information, a modified membership function is defined as follows (Chuang et al., 2006):

$$\mu_{ij}=\frac{\mu_{ij}{}^{q}h_{ij}^{z}}{\sum_{l=1}^{c}\mu_{lj}{}^{q}h_{lj}^{z}} \tag{9}$$

where, $h_{ij}=\sum_{l=\omega_j}\mu_{il}$ is called spatial function; ω_j represents a square window centered on pixel x_j in the spatial domain. The 3×3 and 5×5 windows were used throughout this work. The spatial function h_{ij} represents the probability of belonging the pixel x_j to the i^{th} cluster. The spatial function of a pixel for a cluster is large if the majority of its neighborhood belongs to the same cluster and is small otherwise. q and z are parameters to control the relative importance of both functions. In a homogenous region, the spatial functions simply enhance the original membership and the clustering result remains untouched. However, for a noisy pixel, this formula reduces the weighting of a noisy cluster by the labels of its neighboring pixels. As a result, misclassified pixels from noisy regions can easily be corrected.

Each of the iterations in clustering contains two steps. The first step is the same as that in standard FCM to calculate the membership function in the spectral domain. In the second step, the membership information of each pixel is mapped to the spatial domain and the spatial function is computed. The iteration in FCM proceeds with the new membership incorporating with the spatial function. The iteration is stopped when the maximum difference between two cluster centers at two successive iterations is less than a threshold. After the convergence, defuzzification is applied to assign each pixel to a specific cluster for which the membership is maximal.

SFCM can be described as follows:

Step 1: Set the number of clusters c and the parameter m in (1). Initialize the fuzzy cluster centered vector $V=[v_1, v_2,\ldots, v_c]$, randomly, set $\varepsilon=0.02$, calculate μ_{ij} and v_i by (7) and (8), respectively.

Step 2: Update μ_{ij} and v_i by (9) and (8), respectively.

Step 3: Repeat Step 2 until the following termination criterion is satisfied:

$$\left|v_{new} - v_{old}\right| < \varepsilon \tag{10}$$

3 Cluster validation functions

In order to obtain a quantitative comparison, two types of cluster validation functions, fuzzy partition and feature structure, are often used to evaluate the performance in different clustering methods. The representative functions for the fuzzy partition are: partition coefficient V_{pc} (Bezdek, 1974) and partition entropy V_{pe} (Bezdek, 1975). They are defined as follows:

$$V_{pc} = \frac{\sum_{j=1}^{n}\sum_{i=1}^{c}\mu_{ij}^{2}}{n}$$
$$V_{pe} = \frac{-\sum_{j=1}^{n}\sum_{i=1}^{c}\left[\mu_{ij}\log\mu_{ij}\right]}{n} \tag{11}$$

The idea of these validation functions is that the partition with fuzziness means better performance. As a result, the best clustering is achieved when the value V_{pc} is maximal or V_{pe} is minimal.

The disadvantages of V_{pc} and V_{pe} are that they measure only the fuzzy partition and lack a direct connection to the featuring property. Other validation functions based on the feature structures are available in literature (Fukuyama and Sugeno, 1989; Xie and Beni, 1991). For example, the validation function is defined as follows by Xie and Beni (1991):

$$V_{xb} = \frac{-\sum_{j=1}^{n}\sum_{i=1}^{c}\mu_{ij}\left\|x_j - v_i\right\|^2}{n\times(\min_{i\neq t}\{\left\|v_t - v_i\right\|^2\})} \tag{12}$$

A good clustering result leads to samples compact within a cluster and separated among different ones. Minimizing V_{xb} is expected to result in a good clustering.

The accuracy of an algorithm is computed as follows:

$$Accuracy = \frac{correct\quad segmented\quad pixels}{all\quad of\quad fruit\quad pixels} \tag{13}$$

4 Experimental results

Figure 3 demonstrates the results of the proposed algorithm. The original images are shown in Figure 3a. Figure 3b depicts the manually segmented image. Figure 3c illustrates the segmented images using FCM and without removing stem and calyx. Stem and calyx pixels are classified inversely in the same class with tissue's pixels, since FCM (or SFCM) segments the image pixels through intensity and stem and calyx pixels' intensities resemble the intensity of the tissue. As a solution, the fruit's shape is first extracted from the image using ACM as is shown in Figure 3d. Then, stem and calyx of the fruit are removed using morphological filters as is shown in Figure 3e. Figure 3f depicts the result of FCM. Finally, Figures 3g and 3h show the results for SFCM with 3×3 and 5×5 windows, respectively. As is seen in Figures 3f up to 3h, the accuracy of the algorithm is increased when the stem and the calyx are first removed.

Table 1 shows a quantitative comparison of accuracy and validation functions employed to estimate the efficiency of FCM and also SFCM with 3×3 and 5×5 windows. As is shown in Table 1, the results for SFCM are better than those for FCM.

Table 1 Comparison of the FCM and SFCM algorithms with different windows on the original pomegranate MR images

Method	Accuracy	V_{pc}	V_{pe}	V_{xb} ($\times10^{-3}$)
FCM	98.32	0.9134	0.0760	0.0687
SFCM 3×3	99.52	0.9904	0.0079	0.0627
SFCM 5×5	99.48	0.9904	0.0079	0.0638

The proposed algorithms are also evaluated in a condition with noise interference on pomegranate MR images. Figures 4, 5 and 6 depict the results of the algorithms on MR images corrupted with Gaussian noise (mean = 0 and variance = 0.05), salt and pepper noise with the noise intensity of d = 0.1 and speckle noise with variance = 0.1, respectively. Visually, it is clear that the SFCM (with 3×3 and 5×5 windows) highly outperforms FCM.

Table 2 demonstrates the accuracy and validation functions used in measuring the efficiency of FCM and SFCM algorithms on the images smeared with Gaussian, salt and pepper and speckle noises. As is shown in Table 2, in most cases the validation functions and accuracy for SFCM in the presence of noise are better than those for FCM.

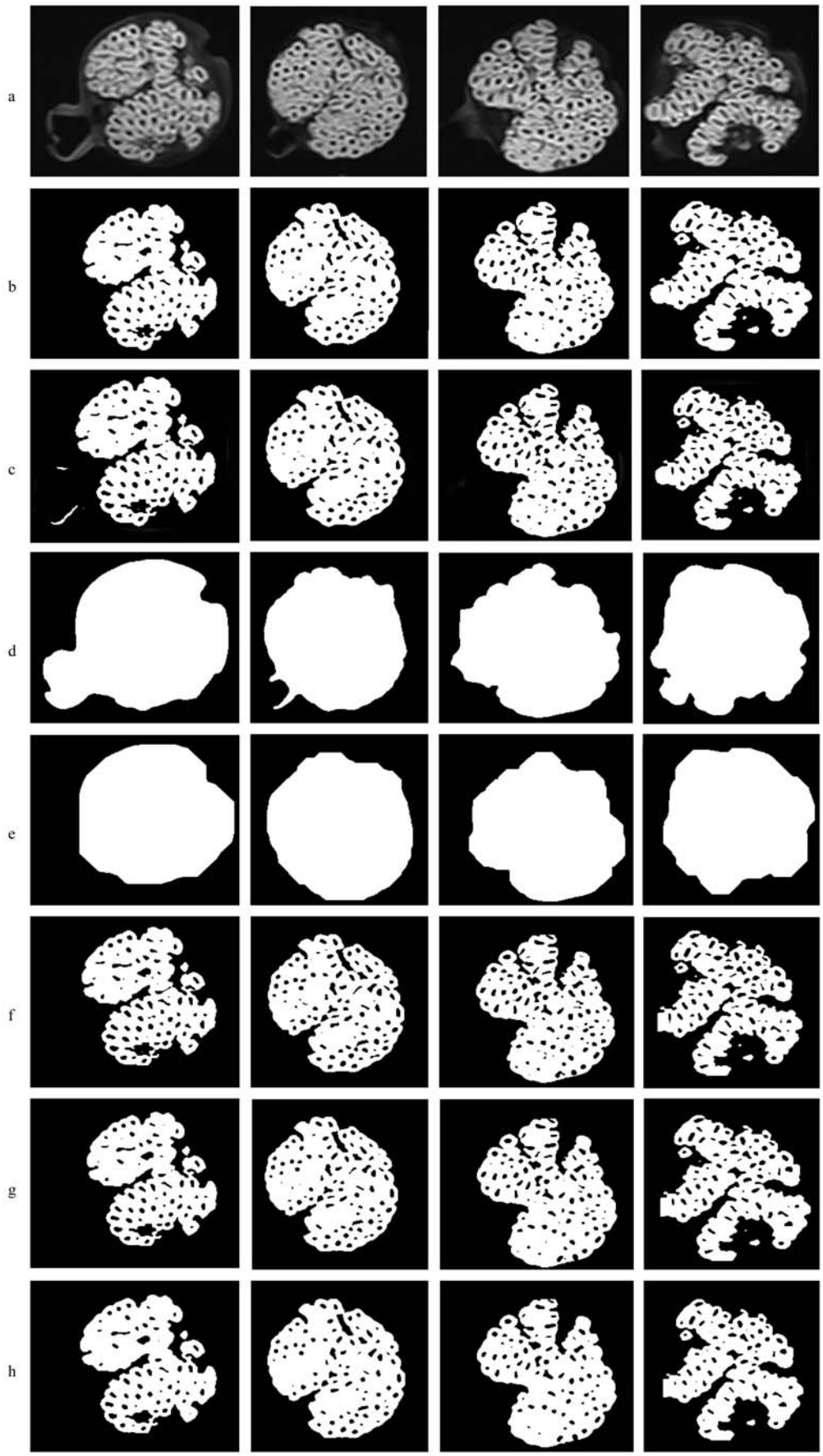

a) Original pomegranate MR images, b) Manually segmented images, c) The segmented images in presence of stem and calyx, d) Shape extraction by ACM algorithm, e) Stem and calyx removing with morphological filters, f) Result of the FCM algorithm, g) Result of the SFCM algorithm with 3×3 window, h) Result of the SFCM algorithm with 5×5 window.

Figure 3 Results of the algorithms on pomegranate MR images

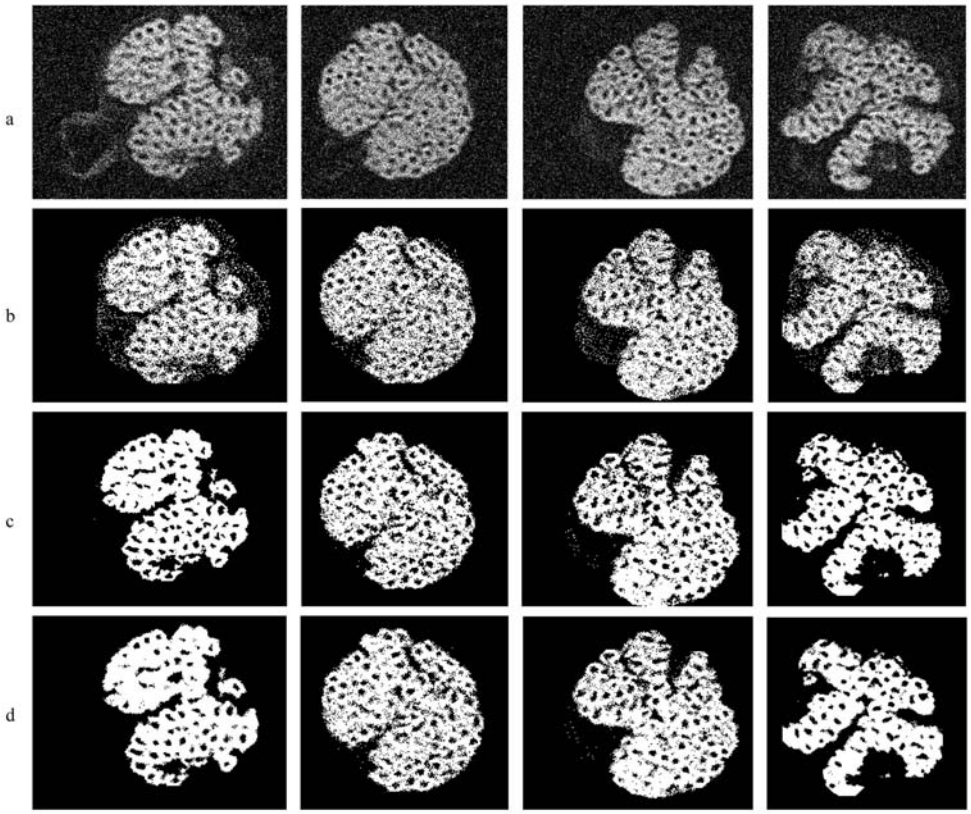

a) Images corrupted by Gaussian noise, b) Images segmented by FCM algorithm, c) Images segmented by SFCM algorithm with 3×3 window, d) Images segmented by SFCM algorithm with 5×5 window

Figure 4 Results of the algorithms on MR images corrupted by Gaussian noise

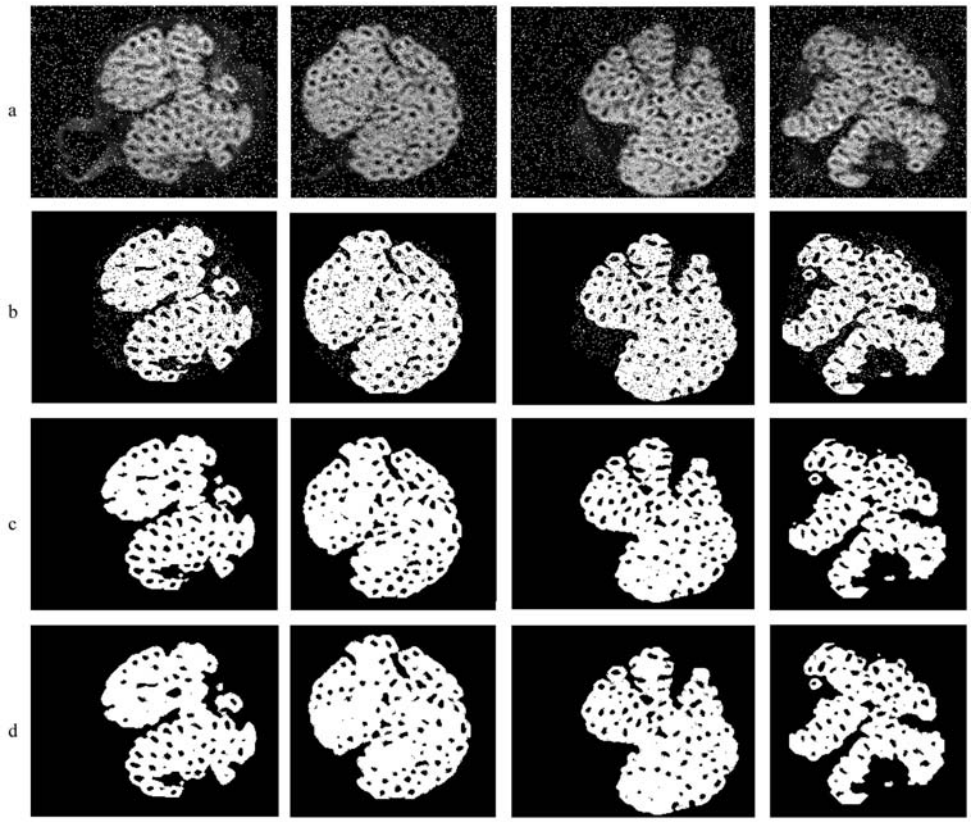

a) Images corrupted by salt and pepper noise, b) Images segmented by FCM algorithm, c) Images segmented by SFCM algorithm with 3×3 window, d) Images segmented by SFCM algorithm with 5×5 window

Figure 5 Results of the algorithms on MR images corrupted by salt and pepper noise

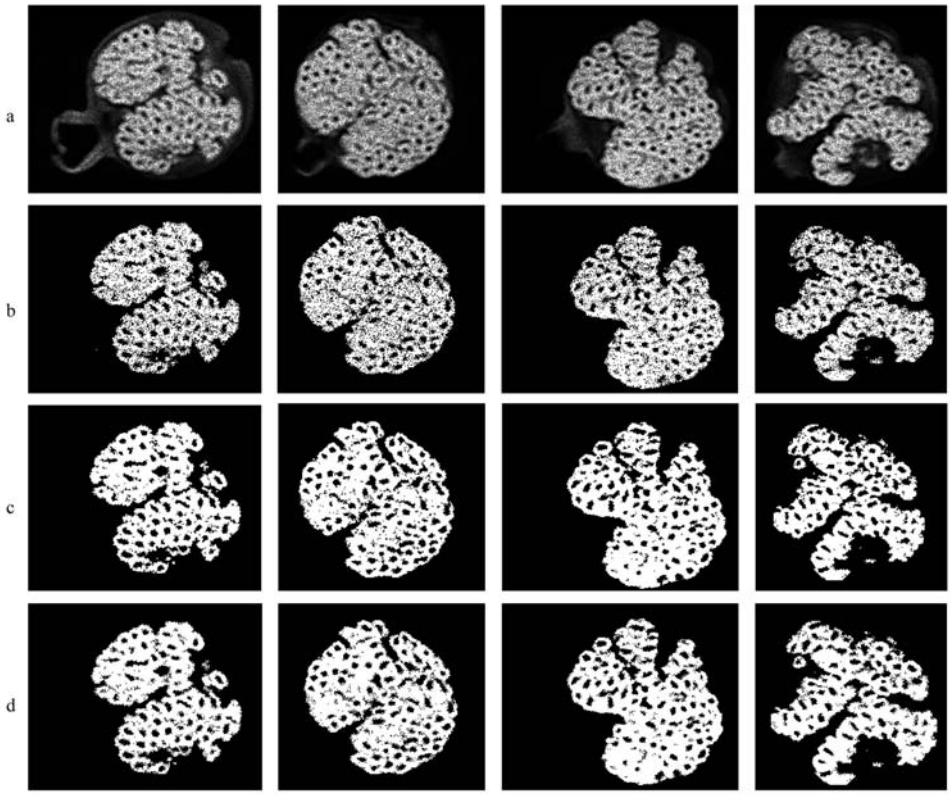

a) Images corrupted by speckle noise, b) Images segmented by FCM algorithm, c) Images segmented by SFCM algorithm with 3×3 window, d) Images segmented by SFCM algorithm with 5×5 window

Figure 6 Results of the algorithms on MR images corrupted by speckle noise

Table 2 Comparison of the FCM and SFCM algorithms with different windows on the pomegranate MR images corrupted with noise

Efficiency measuring method	Gaussian			Salt and pepper			Speckle		
	FCM	SFCM 3×3	SFCM 5×5	FCM	SFCM 3×3	SFCM 5×5	FCM	SFCM 3×3	SFCM 5×5
Accuracy	85.93	95.94	94.9880	95.05	99.49	97.04	98.12	99.85	99.67
V_{pc}	0.8537	0.9525	0.9478	0.8923	0.9737	0.9687	0.8594	0.9352	0.9280
V_{pe}	0.1232	0.0397	0.0437	0.0923	0.0216	0.0257	0.1177	0.0537	0.0593
V_{xb} ($\times 10^{-3}$)	13.6364	9.0006	10.1301	0.0995	0.0340	0.0848	10.8798	8.9096	9.6865

5 Conclusions

In this paper, an automatic algorithm was proposed for segmentation of internal structures of pomegranate into soft tissue and seeds. Since the image pixels are segmented based on their intensity and also because the intensities of stem and calyx are close to the tissue's, in most cases, the stem and calyx are misclassified as internal tissues by the segmentation algorithm. As a solution, the fruit's shape is first extracted from the image using ACM. Then, the stem and calyx are removed by morphological filtering. Finally, an improved version of FCM, SFCM was proposed for segmentation of the pomegranate MR images. This algorithm was realized by incorporating the spatial neighborhood information into the FCM and modifying the membership function of each cluster. The results of SFCM on the original pomegranate MR images and images smeared with Gaussian, salt and pepper, and speckle noise demonstrate that the proposed algorithm is better than FCM algorithm.

Acknowledgements

We would like to thank Dr. Masoud Pour Eisa, Faculty of Medicine, Tabriz University of Medical Sciences, Tabriz, Iran, for providing the pomegranate MR data set taken in Pejvak Imaging Center.

References

Barreiro, P., C. Ortiz, M. Ruiz-Altisent, J. Ruiz-Cabello, M. E. Fernández-Valle, I. Recasens, and M. Asensio. 2000. Mealiness assessment in apples and peaches using MRI techniques. *Magnetic Resonance Imaging,* 17(2): 275-281.

Bezdek, J. C. 1974. Cluster Validity with Fuzzy Sets. *Journal of Cybernetics,* 3(3): 58-72.

Bezdek, J. C. 1975. Mathematical models for systematic and taxonomy. In *Proc. Eigth International Conference on Numerical Taxonomy, G. Estabrook Freeman, San Franscisco, CA*.

Bezdek, J. C. 1981. *Pattern recognition with fuzzy objective function algorithms.* Kluwer Academic Publishers, USA.

Burdon, J., and C. Clark. 2001. Effect of postharvest water loss on 'Hayward' kiwifruit water status. *Postharvest Biology and Technology,* 22(3): 215-225.

Chen, P., J. M. McCarthy, and R. Kauten. 1989. NMR for internal quality evaluation of fruits and vegetables. *Trans ASAE,* 32(5): 1747-1753.

Chuang, K. S., H. L. Tzeng, S. Chen, J. Wu, and T. J. Chen. 2006. Fuzzy c-means clustering with spatial information for image segmentation. *Computerized Medical Imaging and Graphics,* 30(1): 9-15.

Clark, C. J., and D. M. Burmeister. 1999. Magnetic resonance imaging of browning development in 'Braeburn' apple during controlled atmosphere storage under high CO_2. *HortScience,* 34(5): 915-919.

Clark, C. J., J. S. MacFall, and R. L. Bieleski. 1998. Loss of watercore from 'Fuji' apple observed by magnetic resonance imaging. *Scientia Horticulturae,* 73(4): 213-227.

Fadavi, A., M. Barzegar, and M. H. Azizi. 2006. Determination of fatty acids and total lipid content in oilseed of 25 pomegranates varieties grown in Iran. *Journal of Food Composition and Analysis,* 19(6-7): 676-680.

Fukuyama, Y., and M. Sugeno. 1989. A new method of choosing the number of clusters for the fuzzy c-means method. In *Proceedings of fifth fuzzy system symposium, Japan*.

Gonzalez, J., R. C. Valleb, S. Bobroffc, W. V. Biasid, E. J. Mitchamd, and M. J. McCarthyc. 2001. Detection and monitoring of internal browning development in 'Fuji' apples using MRI. *Postharvest Biology and Technology,* 22(2): 179-188.

Kass, M., A. Witkin, and D. Terzopoulos. 1988. Snakes: Active contour models. *International Journal of Computer Vision,* 1(4): 321-331.

Khoshroo, A., A. Keyhani, R. A. Zoroofi, S. Rafiee, Z. Zamani,and M. R. Alsharif. 2009. Classification of pomegranate fruit using texture analysis of MR images. *Agricultural Engineering International: the CIGR Ejournal,* Vol. XI: Manuscript 1182.

Kulkarni, A. P., and S. M. Aradhya. 2005. Chemical changes and antioxidant activity in pomegranate arils during fruit development. *Food Chemistry,* 93(2): 319-324.

Liang, Z. P. and P. C. Lauterbur. 2000. Principles of magnetic resonance imaging; A signal processing perspective. *IEEE Press, New york*.

Moradi, G., M. Shamsi, M. H. Sedaaghi, and M. R. Alsharif. 2010a. Pomegranate MR images analysis using ACM and FCM algorithms. International Conference on Graphic and Image Processing (ICGIP).

Moradi, G., M. Shamsi, M. H. Sedaaghi, and M. R. Alsharif. 2010b. Segmentation of pomegranate MR images using spatial fuzzy c-means (SFCM) algorithm. International Conference on Graphic and Image Processing (ICGIP).

Negi, P. S., G. K. Jayaprakasha, and B. S. Jena. 2003. Antioxidant and antimutagenic activities of pomegranate peel extracts. *Food Chemistry,* 80(3): 393-397.

Nixon, M. S. and A. S. Aguado. 2002. *Feature extraction and image processing*, 1st Edition, Academic Press.

Parvati, K., B. S. Prakasa Rao, and M. Mariya Das. 2008. Image segmentation using gray-scale morphology and marker-controlled watershed transformation. *Discrete Dynamics in Nature and Society,* 2008 (2008): Article ID 384346.

Prabhu Desai, V. G. 1989. Investigation on internal breakdown of pomegranate fruit. Ph.D. Thesis, MPWV, Rahuri.

Saito, K., T. Miki, S. Hayashi, H. Hajikawa, M. Shimada, Y. Kawate, T. Nishizawa, D. Ikegaya, N. Kimura, K. Takabatake, N. Sugiura, and M. Suzuki. 1996. Application of magnetic resonance imaging to non-destructive void detection in watermelon. *Cryogenics,* 36(12): 1027-1031.

Sonego, L., R. Ben-Arie, J. Raynal, and J. C. Pech. 1995. Biochemical and physical evaluation of textural characteristics of nectarines exhibiting woolly breakdown: NMR imaging, X-ray computed tomography and pectin composition. *Postharvest Biology and Technology,* 5(3): 187-198.

Wang, C. Y., and P. C. Wang. 1989. Nondestructive detection of core breakdown in ‘Bartlett’ pears with nuclear magnetic resonance imaging. *Hort Science*, 24(1): 106–109.

Wang, C. Y., P. C. Wang, and M. Faust. 1988. Non-destructive detection of watercore in apple with nuclear magnetic resonance imaging. *Scientia Horticulturae,* 35(3-4): 227-234.

Xie, X. L., and G. Beni. 1991. A Validity Measure for Fuzzy Clustering. *IEEE Trans. Pattern Anal. Mach. Intell,* 3(8): 841-847.

Zion, B., P. Chen, and M. J. McCarthy. 1995. Detection of bruises in magnetic resonance images of apples. *Computers and Electronics in Agriculture,* 13(4): 289-299.